In-Situ and Contactless Evaluation of Performance of Power Converter EMC Filter based on Near-Field Scan Measurement

Alexandre Boyer, Sonia Ben Dhia, Sébastien Serpaud

In-Situ and Contactless Evaluation of Performance of Power Converter EMC Filter based on Near-Field Scan Measurement

A. Boyer, S. Ben Dhia
LAAS-CNRS
Univ. de Toulouse, INSA, UPS, LAAS
Toulouse, France
alexandre.boyer@laas.fr, sonia.bendhia@insa-toulouse.fr

S. Serpaud
IRT Saint-Exupéry institute
Toulouse, France
sebastien.serpaud@irt-saintexupery.com

***Abstract*— This paper presents and validates an original contactless near-field scan-based method to quantify the performance of EMC filter mounted on power converter boards. The proposed method provides indicators about EMC filter attenuation, decoupling capacitor efficiency and differential-mode to common-mode conversion and may help designer to clarify and debug conducted emission issues of power converter boards.**

Keywords— Near-field scan, EMC filter, Conducted emission

I. INTRODUCTION

Power converters constitute one of the main sources of electromagnetic (EM) emission among electronic systems. In order to meet EMC requirements, the reduction of conducted emission (CE) is a major constraint for electronic designers, which requires a careful design of switching cells and EMC filters. Electrical simulation is a typical approach to optimize EMC filtering in order to pass EMC tests without several redesign cycles. However, passing EMC test at the first time remains a challenge because of placement and routing errors and weakness of simulations due to the complexity of a complete EM modeling of electronic systems. A practical solution is a trial-and-error process (i.e. by changing EMC filter components and repeating CE tests until CE compliance is met), but it can be tedious and inefficient if the root-causes of CE have not been identified.

Near-field scan (NFS) is a well-known and powerful tool to diagnose emission source at PCB level, which can provide valuable information to correct board design during prototyping stages without the need of usual and costly EMC facilities [1]. In practice, NFS locates and correlates hot spots of E and H fields in NF region and conducted/radiated emission. However, this analysis remains only qualitative (a direct estimation of CE is not possible) and the identification of a hot spot does not indicate necessarily where and how a design correction has to be brought. These last years, numerous research works have been led to develop processing methods of NFS results, for example to estimate current distribution [2], extrapolate radiated emission [3], or common-mode (CM) CE [4]. Recently, [5] proposes an NFS-based method to quantify the impact of decoupling capacitors on power integrity on an unpowered PCB.

In this paper, this approach is reused and extended for the analysis and diagnosis of CE of power converters. The proposed approach has two major advantages: firstly, it ensures a contactless and in-situ measurement of the attenuation provided by decoupling and filtering components placed on the converter board and, thus, a possible identification of "weak" components and placement-routing errors. Secondly, the measurement is done on unpowered converter, which prevents risks of destruction during NFS of high-voltage power converters. The paper aims at presenting the principles of this approach and validates it through simple case studies. Our purpose is not to propose an alternative method to usual approach to debug CE problems, but rather a complementary method to help designers in complex problems to confirm their analysis with quantitative results and identify solutions more efficiently. The paper is organized as follows: Section II presents the principle of the method and defines the performance indicators. The method can provide a contactless and in-situ measurement of filter attenuation. This property and the formulations derived in Section II are verified in Section III experimentally. In Section IV, the method is tested on a small and simple DC-DC converter in order to prove the correlation between NFS results and CE when EMC filter configuration is changed.

II. PRINCIPLES OF THE APPROACH

The proposed method relies on the coupling between a miniature H near-field probe and a decoupling/filtering capacitor mounted on the power supply of the converter, as illustrated in Fig. 1. The coupling is assumed to be purely magnetic. The excitation of the NF probe, placed just above a capacitor C, generates a differential-mode (DM) source between the power supply lines V+ and V-, as described in Fig. 2. The voltage measured at or upstream the power supply connector on a given load (e.g. at the optionally mounted LISN to account for a typical CE measurement configuration) depends on the attenuation provided by the filtering elements mounted between the excited capacitor and the voltage measurement point. Thus, the measurement of the transfer function between the NF probe and this measurement point, e.g. measured by a vector network analyzer (VNA) on an unpowered converter, can provide an indirect and contactless method to extract the attenuation of an EMC filter mounted within the converter. In the following paragraphs, the theoretical expressions of the transfer function between the NF probe and the power supply terminal are developed in two cases: firstly, the ideal case without any CM impedance (single-ended case) and, secondly the more general case where DM and CM emissions are considered. Moreover, in order to simplify the theoretical analysis, the LISN and its

connection to the power converter are modeled as an equivalent load called Z_{out} placed at the power connector. As this impedance can be characterized by a VNA, it is supposed to be known. Moreover, as the LISN stabilizes the impedance between V+ and V- around 50 Ω, we consider also that Z_{out} is nearly equal to 50 Ω.

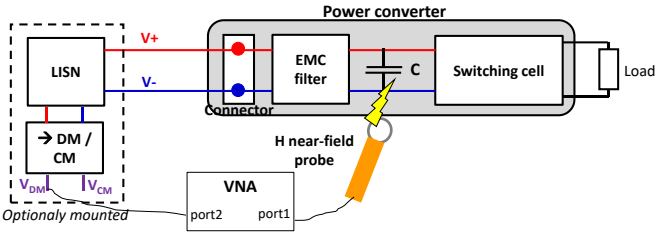

Fig. 1. NFS-based method to measure the attenuation of CE provided by the EMC filter mounted on a power converter

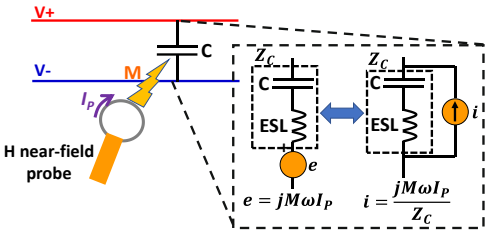

Fig. 2. Differential-mode excitation due to H-field probe coupling on a capacitor mounted on power supply lines

A. *Single-ended case*

In this case, the CE is considered as the voltage measured across Z_{out} at the power connector between the power supply lines V+ and V-. The effect of CM impedance is neglected so that only DM voltage and current are considered. The equivalent model of the NF probe placed above a capacitor C is described in Fig. 3, whose complex impedance is called Z_C which also includes the parasitic inductance due to connections to power supply lines. The mutual inductive coupling M is known, e.g. extracted through a preliminary calibration. The effect of power converter blocks mounted downstream is modeled by an equivalent impedance called Z_{in}'. The effect of all the components mounted between C and the power connector are modeled by a two-port impedance matrix $[Z_f]$ and considered as an EMC filter. The voltage V_{out} at the power connector is measured across Z_{out}.

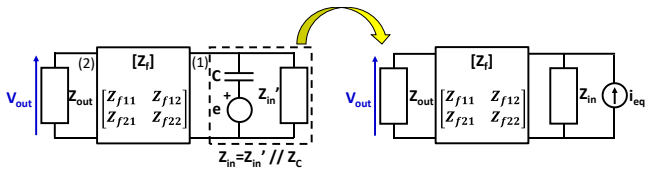

Fig. 3. Equivalent model of the excitation produced by an H-field probe coupled on a capacitor mounted on power suppy lines (single-ended case)

The excitation of the NF probe leads to the generation of a series voltage generator *e*, which depends on *M* and the excitation probe current I_P. According to Fig. 2, the equivalent circuit shown in the right part of Fig. 3 can be built, where i_{eq} is the equivalent current generator due to the H-field coupling and is given by (1). The transfer function between the voltage V_{out} at the power connector and i_{eq}, which characterizes the attenuation provided by the filter between C and the connector, is given by (2). It depends on filter characteristics, but also on power converter and load impedance.

$$i_{eq} = \frac{jM\omega}{Z_C} I_P \quad (1)$$

$$\frac{V_{out}}{i_{eq}} = \frac{Z_{in} Z_{f21} Z_{out}}{(Z_{out}+Z_{f22})(Z_{in}+Z_{f11}) - Z_{f12}Z_{f21}} = \frac{Z_{in} Z_{f21} Z_{out}}{D} \quad (2)$$

The transfer function measured by a VNA between the NF probe and Z_{out} can be expressed by a transmission coefficient S_{21}^P (3), in the case where $Z_{out} = Z_0 = 50$ Ω. This assumption remains acceptable as the LISN used in CE tests has an input impedance close to 50 Ω. The attenuation *Att* provided by the filter modeled by the matrix $[Z_f]$ can be expressed according to (4), and simplifies to (5) if $Z_{in} << Z_{out}$, which is a design target to limit CE. Merging (3) and (5) leads to (6), which expresses S_{21}^P according to the converter input impedance Z_{in} (seen at the coupled capacitor) and filter attenuation.

$$S_{21}^P = 2jM\omega \frac{Z_{in} Z_{f21}}{Z_C D} \quad (3)$$

$$Att = \frac{V_{out}^{filter}}{V_{out}^{no\_filter}} = \frac{Z_{f21}(Z_{in}+Z_{out})}{D} \quad (4)$$

$$Att \approx \frac{Z_{f21} Z_{out}}{D} \quad \text{if } Z_{in} << Z_{out} \quad (5)$$

$$S_{21}^P \approx \frac{2jM\omega}{Z_0} \frac{Z_{in}}{Z_C} Att \quad (6)$$

If the mutual inductance *M* is known (e.g. extract through a prior calibration), its effect on S_{21}^P can be compensated and a first indicator of CE attenuation can be extracted (7). This term depends on two parameters which affect CE:

- The filter attenuation *Att*. A better attenuation reduces S_{21}^P.
- The ratio Z_{in} on Z_C. As explained in [5], this term is a performance indicator of the decoupling provided by C and is useful to compare the performance of several capacitors placed in parallel close together. When Z_C decreases and, hence, becomes a better decoupling element, S_{21}^P tends to increase.

In the case of an adequate placement and routing of C, its impedance Z_C can be estimated with an acceptable accuracy from manufacturer data. Another performance indicator K_{EMC}^P can be extracted according to (8), which gives the transfer impedance between the equivalent current source i_{eq} seen from C and the impedance Z_{out}. A lower value of K_{EMC}^P means a higher attenuation of the CE produced by the power converter.

$$S_{21}^P \frac{Z_0}{2jM\omega} = \frac{Z_{in}}{Z_C} Att \quad (7)$$

$$K_{EMC}^P = S_{21}^P \frac{Z_0 Z_C}{2jM\omega} = Z_{in} Att \quad (8)$$

B. *Extraction of DM noise attenuation*

The previous analysis can be extended when the CM impedances are considered. The transfer function between the NF probe and the DM and CM voltages at the power connectors can be extracted. Fig. 4 describes the equivalent model of the NF probe placed above a capacitor C mounted between power supply lines and the propagation of the DM and CM noise to the power supply connector. The effect of all the components mounted between C and the power connector are modeled by a four-port S-parameter matrix $[S_f]$ and considered as an EMC filter. The voltages on both power supply lines are measured across two identical loads which are supposed to be equal to $Z_0 = 50$ Ω. The excitation of the NF probe leads to the generation of a series voltage generator e, which can be modeled by an equivalent current generator i_{eq}, given by (1), which produces a forward voltage excitation a_1.

In order to study the propagation of DM and CM noise through the EMC filter, it is more convenient to convert [S_f] into mixed-mode representation [S_{MM}].

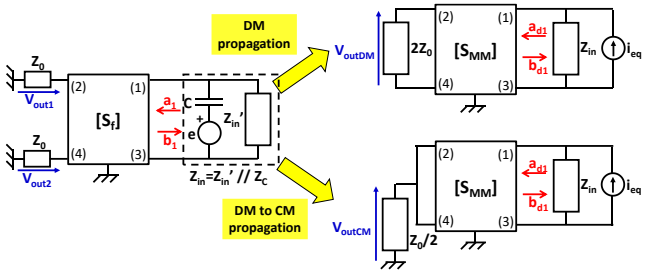

Fig. 4. Equivalent model of the excitation produced by an H-field probe coupled on a capacitor mounted on power suppy lines and propagation of the DM and CM noise to the power supply terminals

As shown in Fig. 4, the equivalent circuit can be transformed into two new equivalent circuits to analyze the propagation of DM and CM noise. In mixed-mode representation, the source produces only a DM excitation, whose forward DM voltage a_{d1} is given by (9), where S_{dd11} is the DM input reflection coefficient of the EMC filter and Z_{dd11} its DM input impedance, extracted from S to Z conversion. The DM voltage at power supply terminals is given by (10) where S_{dd21} is the DM transmission coefficient through the EMC filter. The source induced by NF probe coupling does not generate CM excitation, but CM voltage can be produced on power supply terminal if the EMC filter induces DM to CM conversion. The CM voltage at power supply terminals is given by (11) where S_{cd21} is the DM to CM transmission coefficient through the EMC filter.

$$a_{d1} = Z_{in} i_{eq} \frac{Z_{dd11}}{Z_{dd11}+Z_{in}} \frac{1}{1+S_{dd11}} \quad (9)$$

$$V_{outDM} = Z_{in} i_{eq} \frac{Z_{dd11}}{Z_{dd11}+Z_{in}} \frac{S_{dd21}}{1+S_{dd11}} \quad (10)$$

$$V_{outCM} = Z_{in} i_{eq} \frac{Z_{dd11}}{Z_{dd11}+Z_{in}} \frac{S_{cd21}}{1+S_{dd11}} \quad (11)$$

The DM attenuation Att_{DM} provided by the filter can be expressed by (12), and simplifies if $Z_{in} << 2Z_0$. Similarly, the DM to CM attenuation Att_{DMCM} of the filter can be expressed by (13), and simplifies if $Z_{in} << Z_0/2$. (10) and (11) can be rewritten to (14) and (15), which shows that the transfer function from the NF probe induced excitation and the DM and CM voltage at power terminals depends on EMC filter attenuation.

$$Att_{DM} = \frac{2Z_0+Z_{in}}{2Z_0} \frac{Z_{dd11}}{Z_{dd11}+Z_{in}} \frac{S_{dd21}}{1+S_{dd11}} \approx \frac{Z_{dd11}}{Z_{dd11}+Z_{in}} \frac{S_{dd21}}{1+S_{dd11}} \quad (12)$$

$$Att_{DMCM} = \frac{Z_0/2+Z_{in}}{Z_0/2} \frac{Z_{dd11}}{Z_{dd11}+Z_{in}} \frac{S_{cd21}}{1+S_{dd11}} \approx \frac{Z_{dd11}}{Z_{dd11}+Z_{in}} \frac{S_{cd21}}{1+S_{dd11}} \quad (13)$$

$$V_{outDM} \approx Z_{in} i_{eq} Att_{DM} = jM\omega I_P \frac{Z_{in}}{Z_C} Att_{DM} \quad (14)$$

$$V_{outCM} \approx Z_{in} i_{eq} Att_{DMCM} = jM\omega I_P \frac{Z_{in}}{Z_C} Att_{DMCM} \quad (15)$$

The transmission coefficients S^P_{21DM} and S^P_{21CM} between the NF probe and DM or CM output impedance connected on the power supply terminals at the power converter connector can be expressed by (16) and (17). As in the single-ended case, both transmission coefficients, that can be measured by a VNA, depends on the performance indicator of C (ratio Z_{in}/Z_C) and the DM attenuation or DM to CM attenuation. This measurement offers a contactless method to evaluate the DM attenuation and DM to CM conversion provided by an EMC filter mounted in a power converter.

$$S^P_{21DM} = \frac{2jM\omega}{Z_0} \frac{Z_{in}}{Z_C} Att_{DM} \quad (16)$$

$$S^P_{21CM} = \frac{2jM\omega}{Z_0} \frac{Z_{in}}{Z_C} Att_{DMCM} \quad (17)$$

III. Experimental Validation

In order to validate the expressions presented in Section II, experimental measurements of the coupling between a H near-field probe and capacitors mounted in EMC filter are performed. The purpose of these experiments is to show that the attenuation of the filter can be extracted from the transfer function between the NF probe and the output connector of the filter. The impedances of the components which form the filter are known. As explained in Section II, the extraction of the filter attenuation from the transmission parameter S^P_{21} between the NF probe and the filter output requires the knowledge of the mutual inductive coupling between the probe and the coupled capacitor, in order to compensate this effect. In a first part, the characterization of the mutual inductive coupling is presented.

A. Calibration of the magnetic probe coupling to capacitor

The following experimental set-up is used to extract the mutual inductance M: the tested capacitor is mounted on a test board (with the same technology than the future tested power converter board) and connected to a coaxial connector through a short trace. The H-field probe is placed above the capacitor and the transfer impedance between the probe and the capacitor is measured for different separation distance or scan height between the probe tip and the top of the component case. As long as the H-field probe and the capacitor connection trace are electrically short, the transfer impedance Z^C_{12} is given by (18), which is directly proportional to the mutual inductance *M*.

$$Z^C_{12} = jM\omega \quad (18)$$

The H-field probe consists of a single turn made on a semi-rigid coaxial cable. The diameter of the loop is equal to 5 mm. This proposed set-up was applied for three different X7R ceramic capacitors mounted in SMT packages:

- 50 V 100 nF capacitor mounted in 1206 package (WE 885012208087) – 3.2×1.6×0.8 mm
- 50 V 4.7 µF capacitor mounted in 1206 package (WE 885012208094) – 3.2×1.6×1.6 mm
- 25 V 22 µF capacitor mounted in 1210 package (Murata GRM32ER71E226KE15L) – 3.2×2.5×2.5 mm

The evolution of the transfer impedance between the H-field probe and the 100 nF capacitor is presented in Fig. 5 for separation distances ranging from 0.5 and 5 mm. As expected, the transfer impedance increases linearly with frequency and decreases with the separation distance. *M* can be extracted for each separation distance as shown in Fig. 6. The same experiment has been repeated for the two other capacitors and the results are plotted in Fig. 6. Obviously, *M* depends on the scan height, but also on the capacitor thickness, since a thicker capacitor leads to a larger separation between the probe and the board.

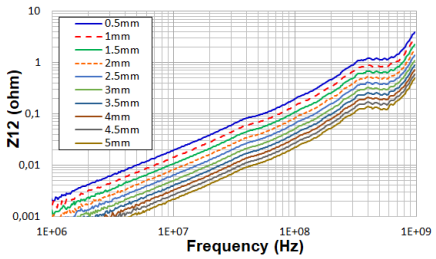

Fig. 5. Measurement of the transfer impedance between the H-field probe and the 100 nF capacitor for various scan height

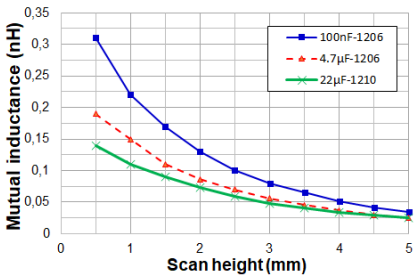

Fig. 6. Extraction of the mutual inductance between the tested ceramic capacitors and the H-field probe vs. the separation distance

B. *Extraction of the attenuation of a single-ended EMC filter*

In order to test the validity of the indirect evaluation of EMC filter attenuation based on NFS measurement, the method is used to estimate the attenuation provided by a CLC pi-filter terminated by known loads: here 50 Ω. In a first case study, a single-ended CLC filter is considered. It is made of a SMT 22 µH shielded inductor (WE-PD 7447715220) and two 100 nF ceramic capacitors tested in III.A. The EMC filter is mounted on a two-layer test board and terminated on both sides by SMA connectors. The H-field probe is placed at 1 mm above the input capacitor of the filter, whose input terminal is loaded by a 50 Ω load, as illustrated in Fig. 7.

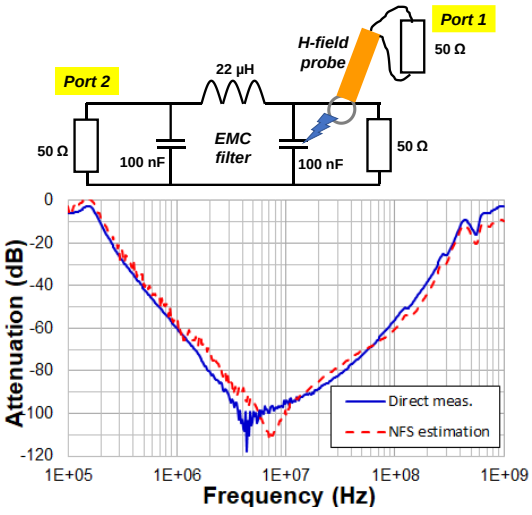

Fig. 7. Indirect measurement of the attenuation of an EMC filter: experimental set-up (top) and comparison between the direct and indirect measurement of the filter attenuation (bottom)

The coupling between the H-field probe and the output of the filter is measured by a Vector Network Analyzer (VNA). In order to increase the dynamic range of the VNA, a low-noise amplifier (LNA) with a gain of 30 dB is connected at the output of the NF probe. According to (6), as the ceramic capacitor and the input impedances are known, the attenuation of the EMC filter ended by 50 Ω loads can be extracted. It is also compared with the direct measurement of the attenuation measured by a VNA connected between the two terminals of the filter. Fig. 7 shows the comparison between the results of both methods which are in good agreements. The differences, especially visible around the maximum attenuation frequency, can be explained by uncertainties about input capacitor impedance and mutual inductive coupling.

C. *Extraction of the attenuation of a differential EMC filter*

In a second case study, the previous experiment is repeated on a differential second-order EMC filter. The filter is made of a SMT CMC (WE-UCF 744290472), two 100 nF ceramic capacitors (C_{Y1} and C_{Y2}) and a 4.7 µF ceramic capacitors (C_X), also tested in III.A. All the terminals of the filter are loaded by 50 Ω loads, as illustrated in Fig. 8. A small amount of dissymmetry is voluntary added in the placement of C_{Y1} and C_{Y2}, leading to different parasitic inductances L_{P1} and L_{P2}, in order to increase the DM-to-CM conversion.

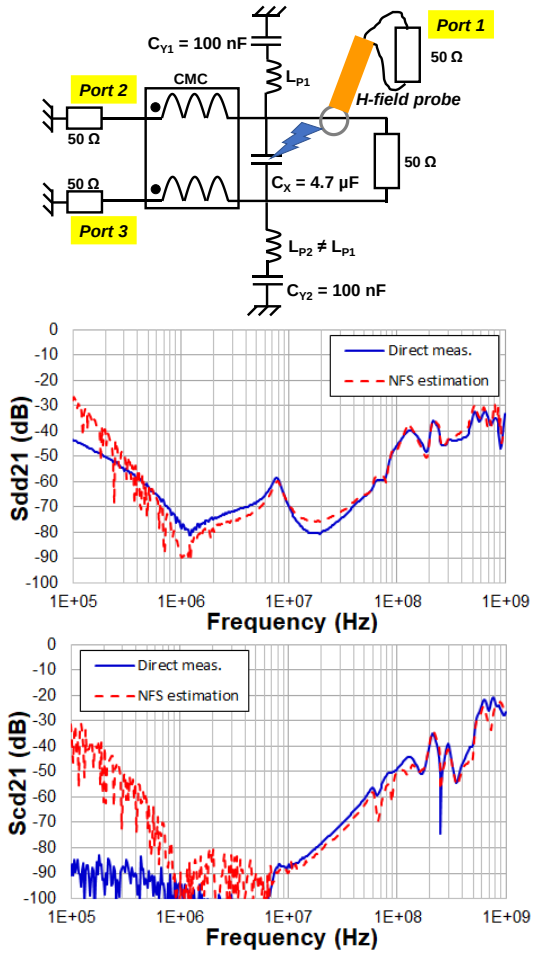

Fig. 8. Indirect measurement of the attenuation of a differential EMC filter: experimental set-up (top) and comparison between the direct and indirect measurement of the DM attenuation (middle) and DM-to-CM conversion (bottom)

The filter is characterized initially with a four-port VNA and its DM-to-DM attenuation and DM-to-CM conversion are extracted, given by the mixed-mode S-parameters Sdd21 and Scd21. Then, the H-field probe is placed at 1 mm above the 4.7 µF capacitor and the coupling to the ports 2 and 3 are measured. The Sdd21 and Scd21 parameters of the EMC filter are extracted from NF measurements based on (16) and (17), knowing the differential load impedance. Fig. 8 presents the

comparison between the direct and indirect measurements of Sdd21 and Scd21, which are in good agreements. The differences visible below 1 MHz are explained by the insufficient dynamic range of the VNA.

IV. Analysis of a DC-DC converter

The proposed approach is tested on a small power converter board. It consists of a buck synchronous converter designed around the LT3800 controller, which converters 12 V to 5 V. The simplified schematic is presented in Fig. 9, which gives details on the power input stage. It is designed around the local decoupling of the switching (SW) cell (C_{IN1} to C_{IN3}) and an EMC filter (L_F, C_{F1} and C_{F2}) whose components are mounted optionally. The power converter is connected to the 12 V power sources through a 1.2 m long cable routed at 5 cm above a conductive reference plane and a (50 µH+5 Ω)//50 Ω CISPR-LISN in order to measure the DM noise in a typical CE test. In parallel, the proposed NFS-based approach to diagnose CE is applied on the power converter board, in order to correlate NFS results with the direct measurement of CE. The DC-DC converter is unpowered. The coupling between the H-field probe (same probe used in Section III) and a SMA connector mounted on the power supply terminal is measured by a VNA. The 1.2 m power cable is not mounted. A 30 dB LNA is placed at the NF probe output to increase the dynamic range. The NF probe is placed at 1 mm above C_{IN1}, C_{F1} or C_{F3}.

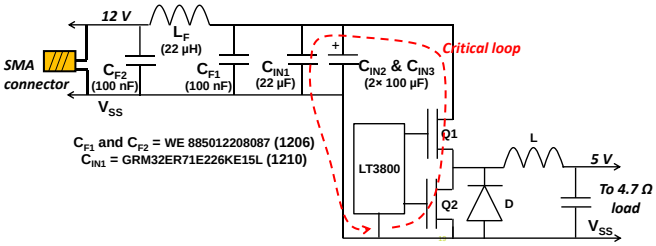

Fig. 9. Schematic of the tested power converter

A. Analysis of the effects of the filtering capacitors

In a first experiment, only C_{F1} and C_{F2} are mounted in the EMC filter and the CE is measured (Fig. 10). NFS are also done with the probe coupled on C_{IN1}, C_{F1} and C_{F2}. The three measured transmission coefficients S_{21}^P are processed: firstly, as the mutual inductance is known, the effect of inductive coupling is compensated as given by (7) (indicator $S_{21}^P/M\omega$). Secondly, as the capacitors is routed as close as possible to the power supply rails, the parasitic inductance due to capacitor connections remains small. VNA measurements of these capacitors provide a good estimation of their impedance. Thus, the indicators K_{EMC}^P can be extracted with a good confidence. Both indicator types are plotted in Fig. 11.

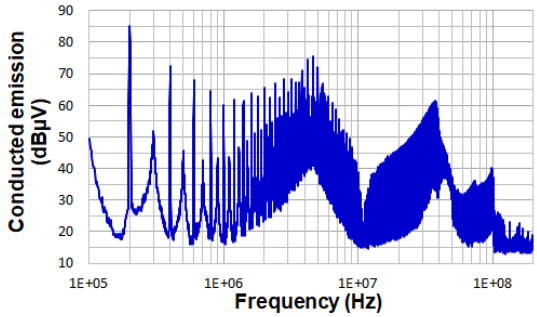

Fig. 10. Conducted emission produced by the DC-DC converter with an EMC filter formed by C_{F1} and C_{F2} (L_F removed)

K_{EMC}^P is actually the transfer impedance between the coupled capacitor and the power connector. As C_{IN1} is placed close to the SW cell, it quantifies the attenuation between the SW cell and the power connector. Comparing Figs. 10 and 11 shows a correlation between CE level and K_{EMC}^P: two local minima are visible at 1.2 and 12 MHz and a local maximum is visible at 4.6 MHz, related to capacitor resonances and antiresonances. The CE spectrum shows also a major peak at 37 MHz, which is due to the resonance of the critical loop formed by the SW cell and the decoupling capacitors. However, this resonance is not visible on K_{EMC}^P, but two resonances appears at 24 and 43 MHz instead. They are also related to the critical loop but the shift is explained by the difference of SW cell between powered and unpowered converter.

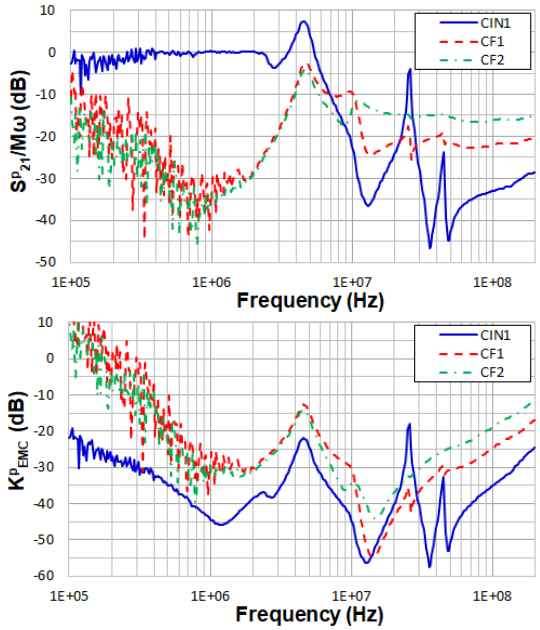

Fig. 11. Comparisons of the indicators $S_{21}^P/M\omega$ (top) and K_{EMC}^P (bottom) measured over the capacitors C_{IN1}, C_{F1} and C_{F2}

The roles of C_{IN1}, C_{F1} and C_{F2} can be appreciated by the comparison of the indicator $S_{21}^P/M\omega$, which depends on EMC filter attenuation and decoupling efficiency (7). Up to several MHz, the EMC filter does not provide significant attenuation, and the decoupling efficiency of the three capacitors can be compared. As the indicator is maximal for C_{IN1}, it contributes mostly to the SW cell decoupling in this frequency range. The influence of C_{F1} and C_{F2} is identical and tends to increase with frequency. A common antiresonance of these capacitors is clearly visible at 4.6 MHz. Above several MHz, the EMC filter attenuation is not negligible and the comparison between C_{IN1} and C_{F1} or C_{F2} is not possible anymore as they are separated by few centimeters. It is interesting to notice that the resonances at 24 and 43 MHz are very strong above C_{IN1}, but weak above C_{F1} and nearly imperceptible above C_{F2}, proving that C_{IN1} is involved in these resonances contrary to C_{F1} and C_{F2} which contributes to filter them. Above several tens of MHz, K_{EMC}^P is larger for C_{F2} than C_{F1} and C_{IN1} as C_{F2} is placed close to the power connector. This ascending succession is a sign of an adequate EMC filter implementation.

B. Comparison between different filter topologies

In a second experiment, the CE emission produced by the converter is measured with different input EMC filter configurations: without EMC filter, with only C_{F1}, only L_F,

only C_{F1} and L_F, only L_F and C_{F2}. The measured CE spectrum envelops are compared in Fig. 12. The coefficient S_{21}^P is also measured with the NF probe placed above C_{IN1} and process to get the indicator K_{EMC}^P. They are compared for the different EMC filter versions in Fig. 13. Results below 300 kHz are not relevant due to the sensitivity limits of the VNA.

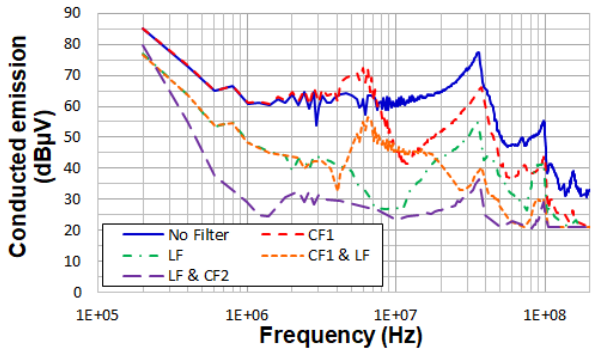

Fig. 12. Comparison of CE spectrum envelops produced by the DC-DC converter for different filter configurations

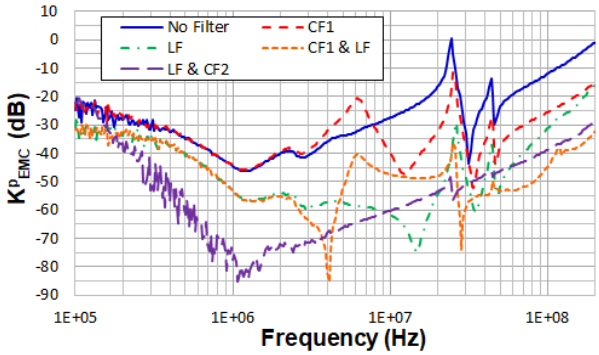

Fig. 13. Comparison of indicators K_{EMC}^P extracted from NFS measurement above C_{IN1} for different filter configurations

Compared to the version without filter, adding C_{F1} reduces CE above 7 MHz, with a level reduction that reaches 20 dB at 12 MHz and about 10 dB above 50 MHz. However, this filter configuration makes CE worse between 3 and 7 MHz, introducing an increase of 10 dB. Very similar observations can be made with the indicators K_{EMC}^P. They are identical up to 3 MHz, showing that C_{F1} has no effect on CE up to this frequency, but K_{EMC}^P measured with C_{F1} exceeds the one measured without filter between 3 and 8 MHz up to 12 dB. Above 8 MHz, it decreases compared to the version without filter: up to 22 dB at 22 MHz and 12 dB above 50 MHz. Introducing only L_F has a better effect on CE compared to a filter based on C_{F1}. Compared to the version without filter, the CE reduction reaches about 8 dB at 200 kHz, 12 dB at 1 MHz, 32 dB at 10 MHz and between 12 and 23 dB above 30 MHz. The comparison of K_{EMC}^P shows similar trends with a reduction of 10 dB at 1 MHz, 34 dB at 10 MHz and between 20 and 25 dB above 30 MHz. Whereas the K_{EMC}^P reduction is nearly stable above 30 MHz, it is not the case with CE reduction because of the effect of resonances of power cable, which was not connected during NFS.

With both LF and CF1 filter configuration, the presence of a major resonance at 37 MHz due to the critical loop is clearly visible in the CE spectrum and K_{EMC}^P curves as well. Adding C_{F1} to L_F degrades the EMC filter efficiency between 4.5 and 20 MHz, with an increase of up to 20 dB of the CE. The same degradation arises on K_{EMC}^P curves, where the adding of C_{F1} leads to an increase ranging from 10 to 20 dB between 4.5 and 25 MHz. Adding C_{F1} reduces CE by nearly 15 dB above 20 MHz. A similar reduction is also visible with K_{EMC}^P curves, as well as a less pronounced resonance due to the critical loop. The best filter configuration is the L_F – C_{F2} combination which leads to a CE reduction of 30-35 dB between 1 and 10 MHz and about 20-25 dB above 50 MHz compared to the version without filter. A similar trend is measured with K_{EMC}^P, with a reduction of 30-32 dB between 1 and 10 MHz, and 20-25 dB above 50 MHz. An important attenuation of the resonances at 24 and 43 MHz appears on K_{EMC}^P, which is correlated with the strong attenuation of the critical loop resonance in the CE spectrum.

In spite of local differences due to power cable resonances and SW cell impedance changes in the powered converter, these results exhibit a clear correlation between the CE level and K_{EMC}^P changes. They prove that the proposed NFS-based method captures the improvement and/or degradation of EMC filter and decoupling cells, providing a potential method to diagnose EMC problems of power converters.

V. Conclusion

This work has presented and validated an original contactless NFS-based method to quantify the performance of EMC filter mounted on power converter applications. The method relies on the local coupling between a magnetic NF probe and a capacitor mounted between the power supply lines in order to generate DM excitation. Applied on an unpowered board, indicators about filter attenuation, decoupling efficiency and DM-to-CM conversion can be extracted, if a careful calibration of the probe coupling on capacitor has been done previously. Compared to traditional approach to debug CE problems, one advantage of this approach is that the influence of the different filtering capacitors can be appreciated by changing the position of the NF probe, offering a deeper analysis and possible identification of the origin of CE problems. Futures works will clarify how these indicators extracted by this method can help CE debugging on more complex power converters. Moreover, the method should be updated to be applied on powered converters as the filter performance may change with biasing.

References

[1] IEC 61967-3, TS, Ed.1: Integrated circuits- Measurement of electromagnetic emissions, 150 kHz to 1 GHz - Part 3: Measurement of radiated emissions – Surface scan method.

[2] H. Weng, D. G. Beetner, R. E. DuBroff, J. Shi, “Estimation of High-Frequency Currents From Near-Field Scan Measurements”, IEEE Trans. on EMC, vol. 49, no. 4, Nov. 2007.

[3] X. Tong, D. W. P. Thomas, A. Nothofer P. Sewell, C. Christopoulos, “Modeling Electromagnetic Emissions From Printed Circuit Boards in Closed Environments Using Equivalent Dipoles”, IEEE Trans. on EMC, vol. 52, no. 2, May 2010.

[4] A. Boyer, N. Nolhier, F. Caignet, S. Ben Dhia, “Anticipating Common-Mode Conducted Emission of DC-DC Converter from Electric Near-Field Scan”, 2021 Joint IEEE Intl Symp. On EMC, SI & PI, and EMC Europe, Aug. 2021.

[5] S. Serpaud, "Application de la méthode de mesure champ proche en émission pour l’aide à la conception et à l’investigation des non-conformités CEM des cartes électroniques", Ph.D. dissertation, INSA Toulouse, Univ. of Toulouse, Toulouse, France, 2023.